

# Neutron spectroscopy and magnetic relaxation of the Mn<sub>6</sub> nanomagnets.

S. Carretta<sup>1</sup>, T. Guidi<sup>2</sup>, P. Santini<sup>1</sup>, G. Amoretti<sup>1</sup>, O. Pieper<sup>3,4</sup>, B. Lake<sup>3,4</sup>, J. van Slageren<sup>5,6</sup>, F. El Hallak<sup>5</sup>, W. Wernsdorfer<sup>7</sup>, H. Mutka<sup>8</sup>, M. Russina<sup>3</sup>, C.J. Milios<sup>9</sup> and E. K. Brechin<sup>9</sup>

<sup>1</sup> *Dipartimento di Fisica, Università di Parma, I-43100 Parma, Italy*

<sup>2</sup> *ISIS Pulsed Neutron Facility, Rutherford Appleton Laboratory, Chilton, OX11 0QX, United Kingdom*

<sup>3</sup> *Hahn-Meitner Institut, Glienicker Strasse 100, 14109 Berlin, Germany*

<sup>4</sup> *Institut für Festkörperphysik, Technische Universität Berlin, 10623 Berlin, Germany*

<sup>5</sup> *1. Physikalisches Institut, Universität Stuttgart, D-70550 Stuttgart, Germany*

<sup>6</sup> *School of Chemistry, University of Nottingham, Nottingham NG7 2RD, United Kingdom*

<sup>7</sup> *Laboratoire Louis Néel-CNRS, F-38042 Grenoble Cedex, France*

<sup>8</sup> *Institute Laue-Langevin, B.P. 156, F-38042 Grenoble Cedex, France and*

<sup>9</sup> *University of Edinburgh, West Mains Road, Edinburgh, EH9 3JJ, U.K.*

(Dated: November 2, 2018)

Inelastic neutron scattering has been used to determine the microscopic Hamiltonian describing two high-spin variants of the high-anisotropy Mn<sub>6</sub> nanomagnet. The energy spectrum of both systems is characterized by the presence of several excited total-spin multiplets partially overlapping the S=12 ground multiplet. This implies that the relaxation processes of these molecules are different from those occurring in prototype giant-spin nanomagnets. In particular, we show that both the height of the energy barrier and resonant tunnelling processes are greatly influenced by low-lying excited total-spin multiplets.

PACS numbers: 75.50.Xx, 75.40.Gb, 75.60.Jk, 78.70.Nx

Keywords : Molecular magnets, Neutron inelastic scattering, Dynamic properties , Magnetization reversal mechanisms

## I. INTRODUCTION

Molecular nanomagnets (MNM) have recently attracted considerable interest because at low temperature  $T$  they display slow relaxation of the magnetization  $M$  of purely molecular origin [1]. The main relaxation mechanism is provided by the interactions of the spin degrees of freedom with phonons, either through modulation of the local crystal fields on individual magnetic ions, or through modulation of two-ion interactions. Typically, the relaxation dynamics are modelled by restricting the spin Hilbert space to the ground total-spin multiplet only, as resulting from the usually dominating isotropic exchange interactions. In this framework, each  $N$ -spins molecule is described as a single giant spin  $S$  in an effective crystal-field potential. At temperatures of few K, the reversal of  $M$  occurs through a multi-step Orbach process yielding a thermally activated behavior of the relaxation time,  $\tau = \tau_0 \exp(U/k_B T)$ , where the energy barrier  $U$  is set by the effective axial anisotropy experienced by the giant spin [2].

We show that excited  $S$ -multiplets strongly influence the energy barrier for the relaxation of  $M$  in two high-spin ( $S = 12$ ) variants of the high-anisotropy Mn<sub>6</sub> nanomagnet (a record barrier  $U = 86.4$  K, and  $U = 53.1$  K [3, 4]). In fact, inelastic neutron scattering (INS) and Frequency Domain Magnetic Resonance Spectroscopy

(FDMRS) show that the two variants are characterized by a similar anisotropy but have significantly different exchange interactions. The large difference in  $U$  is mainly due to the presence of relaxation paths passing through excited  $S$  multiplets partially nested within the ground one. In addition, because of  $S$ -mixing in the wavefunctions, these excited manifolds may lead to resonant inter-multiplet tunnelling processes for fields of a few thousands of Gauss. These are associated with additional steps in hysteresis cycles which are absent in the giant spin model.

## II. SPIN HAMILTONIAN AND MOLECULAR ENERGY LEVELS

The two Mn<sub>6</sub> molecules have chemical formula Mn<sub>6</sub>O<sub>2</sub>(Et-sao)<sub>6</sub>(O<sub>2</sub>CPh(Me)<sub>2</sub>)<sub>2</sub>(EtOH)<sub>6</sub> (higher barrier) and Mn<sub>6</sub>O<sub>2</sub>(Et-sao)<sub>6</sub>(O<sub>2</sub>CPh)<sub>2</sub>(EtOH)<sub>4</sub>(H<sub>2</sub>O)<sub>2</sub> (lower barrier) and are nearly isostructural. The magnetic core comprises six Mn<sup>3+</sup> ions arranged on two triangles bridged by oxygen atoms (Fig. 1). Each Mn<sup>3+</sup> ion has a distorted octahedral cage of ligands, with the Jahn–Teller axes all approximately perpendicular to the planes of the triangles. The six Mn<sup>3+</sup> ions have spin  $s = 2$  and are coupled by dominant ferromagnetic interactions, leading to a high  $S = 12$  total-spin ground state, as can be inferred by magnetization measurements, see Fig. 2 [3, 4].

Each Mn<sub>6</sub> molecule can be described by the following spin Hamiltonian [5]

$$H = \sum_{i < j} J_{ij} \mathbf{s}(i) \cdot \mathbf{s}(j) + \sum_i d_i s_z^2(i) +$$

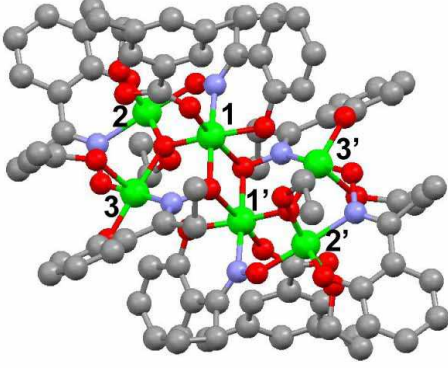


FIG. 1: (color online) Structure of the high-barrier  $\text{Mn}_6$  molecule (H omitted for clarity). Green : Mn, red : O, blue : N, dark grey : C).

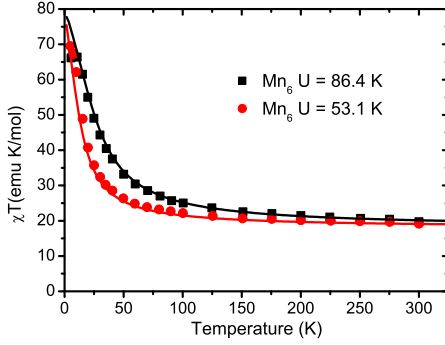


FIG. 2: (color online) Measured (points) and calculated (lines)  $T$ -dependence of the susceptibility for the two  $\text{Mn}_6$  molecules. Calculations are made by including exchange interactions only, with the parameters determined by INS.  $g = 2$  has been assumed.

$$\sum_i c_i (35s_z^4(i) + (25 - 30s(s+1))s_z^2(i)) + g\mu_B \mathbf{B} \cdot \mathbf{S} + H', \quad (1)$$

where  $s(i)$  are spin operators of the  $i^{\text{th}}$  Mn ion and  $\mathbf{S} = \sum_i s(i)$  is the molecule's total spin. The first term is the isotropic exchange, while the second and third terms describe axial local crystal-fields (a  $z$  axis perpendicular to the triangles plane is assumed), and  $\mathbf{B}$  is the external field[1].  $H'$  (neglected in the following) represents additional small anisotropic terms. The minimal set of free parameters is given by three different exchange constants  $J_{11'} \equiv J_1$ ,  $J_{12} = J_{23} = J_{13} = J_{1'2'} = J_{2'3'} = J_{1'3'} \equiv J_2$ , and  $J_{13'} = J_{1'3} \equiv J_3$  (Fig.1) and two sets of crystal-field (CF) parameters  $d_1 = d_{1'}$ ,  $c_1 = c_{1'}$ , and  $d_2 = d_{2'}$ ,  $c_2 = c_{2'}$ . The ligand cages of sites 1 and 3 are rather similar and we assumed the corresponding CF parameters to be equal. Since experimental information is insufficient to fix independently the two small  $c$  parameters, we have chosen to constrain the ratio  $c_1/c_2$  to the ratio  $d_1/d_2$ . The anisotropic terms break rotational invariance and

here lead to a large amount of mixing of different  $S$  multiplets ( $S$  mixing [6]). In the following we label the states by their leading  $S$ -component.

To determine the parameters appearing in (1), we

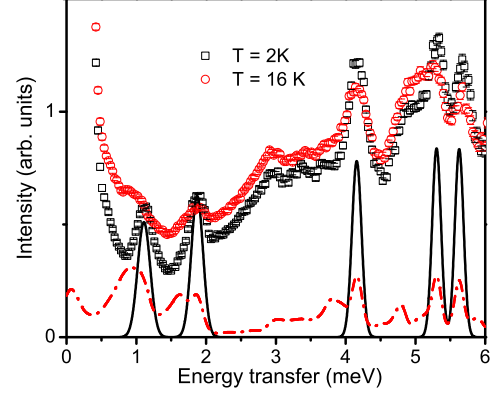


FIG. 3: (color online) INS spectra for the higher barrier molecule collected on IN5 with incident wavelength of 3.4 Å for  $T = 2$  K (black) and  $T = 16$  K (red). Lines are theoretical calculations with model (1).

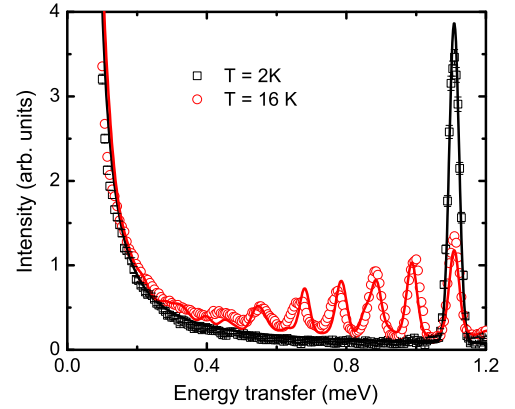


FIG. 4: (color online) INS spectra for the higher barrier molecule collected on IN5 with incident wavelength of 6.7 Å for  $T = 2$  K (black) and  $T = 16$  K (red). Lines are theoretical calculations with model (1).

have used the time-of-flight neutron spectrometers NEAT at the Hahn Meitner Institut (Berlin) and IN5 at the Institute Laue Langevin (Grenoble). In addition, we have performed FDMRS measurements at the University of Stuttgart. Since FDMRS is sensitive to intra-multiplet transitions only, its use in conjunction with INS makes easier to assess the character of the different observed excitations. Figs. 3 and 4 show examples of INS spectra together with theoretical simulations.

The analysis of INS and FDMRS data leads to the following parameters for the higher (lower) barrier compounds :  $J_1 = -0.84(-0.61)$  meV,  $J_2 = -0.59(-0.31)$  meV,  $J_3 = 0.01(0.07)$  meV,  $d_1 = -0.20(-0.23)$  meV,  $d_2 = -0.76(-0.97)$  meV and  $c_1 = -0.001(-0.0008)$  meV [5]. These parameters are consistent with susceptibility measurements (see Fig. 2). Hence, anisotropy is similar in the two variants whereas the dominant ferromagnetic exchange is substantially larger in the higher-barrier compound. Figures 5 and 6 show the energies of the  $S$ -multiplets resulting from the exchange part of (1). It is evident from these figures that the exchange splitting between the ground  $S = 12$  manifold and many excited multiplets, including low- $S$  ones, is smaller than the energy scale of anisotropic terms in (1). In particular, Fig. 6 shows that in the lower-barrier compound the energy of the lowest-lying  $S = 0$  multiplet is only about 4 meV larger than that of the ground one. Thus, the

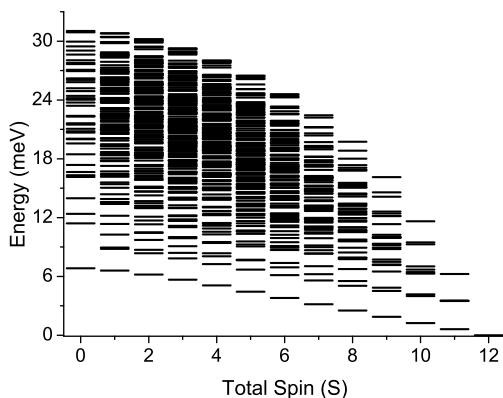


FIG. 5: Energy of all  $S$ -multiplets for the higher barrier compound, resulting from the exchange part of (1) with the parameters given in the text.

giant spin mapping completely breaks down in these two molecules, not only for the large  $S$ -mixing in the wavefunctions, but even for failing to account for the number of states located below the barrier. The presence of a center of inversion (characterizing the structure determined at 150 K) implies that exchange multiplets can be classified according to their parity with respect to the associated spin-permutation operation. For instance, the ground  $S = 12$  states are even, whereas the lowest-lying  $S = 11$  states are odd.

### III. RELAXATION OF THE MAGNETIZATION

The main difference between the two  $\text{Mn}_6$  variants is the position of the excited  $S$  manifolds, therefore the comparison between the relaxation behavior of these systems offers the opportunity to study the role played by low-lying excited multiplets. To address this issue, we

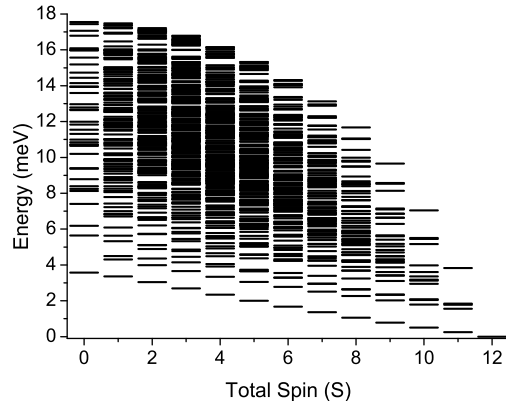


FIG. 6: Energy of all  $S$ -multiplets for the lower barrier compound, resulting from the exchange part of (1) with the parameters given in the text.

adopt the well established framework presented in [7, 8] for the irreversible evolution of the density matrix  $\rho(t)$ . By focusing on time scales much longer than the typical periods of free evolution of the system, the so-called secular approximation enables the time evolution of the diagonal matrix elements of the density matrix to be decoupled from that of the off-diagonal ones. In particular, the populations of the molecular eigenstates,  $p_l(t)$ , evolve through master equations:

$$\dot{p}_l(t) = \sum_m W_{lm} p_m(t), \quad (2)$$

where  $W_{lm}$  is the  $lm$  element of the rate matrix, i.e., the probability per unit time that a transition between levels  $|m\rangle$  and  $|l\rangle$  is induced by the interaction with the phonon heat bath. The latter can be calculated by perturbation theory once magnetolelastic (ME) interactions have been modelled. Experimental information is totally insufficient to fix all the many possible parameters appearing in the ME coupling potential. By assuming that the main contribution to this coupling arises from the modulation of the local rank-2 crystal fields and that quadrupole moments of each individual Mn ion are isotropically coupled to Debye acoustic phonons, we obtain [9]

$$W_{lm} = \gamma^2 \Delta_{lm}^3 n(\Delta_{lm}) \sum_{i,j,q_1,q_2} \langle l | O_{q_1,q_2}(\mathbf{s}_i) | m \rangle \times \langle m | O_{q_1,q_2}(\mathbf{s}_j) | l \rangle, \quad (3)$$

where  $i$  and  $j$  run over Mn ions,  $O_{q_1,q_2}(\mathbf{s}_i)$  are the components of the cartesian quadrupole tensor operator,  $n(x) = (e^{\hbar x/k_B T} - 1)^{-1}$  and  $\Delta_{lm} = (E_l - E_m)/\hbar$ . The single free parameter  $\gamma$  is proportional to the ME coupling strength. In spite of the complexity of their energy spectrum, for both variants the resulting relaxation spectrum

at low  $T$  is dominated by a *single* relaxation time displaying a nearly Arrhenius behavior  $\tau(T) = \tau_0 \exp(U/K_B T)$ , in agreement with experiments [5]. In particular, the effective energy barrier for the magnetization reversal is crucially dependent on the position of low-lying excited  $S$  multiplets. Indeed, the large difference between the barriers of the two molecules mainly results from the variation of the ferromagnetic exchange constants and not from a variation in anisotropy. It is also worth to note that in the present case  $U$  is not set by the energy of the lowest-lying  $M_S = 0$  state as one could naively expect.

The existence of several total-spin multiplets partially

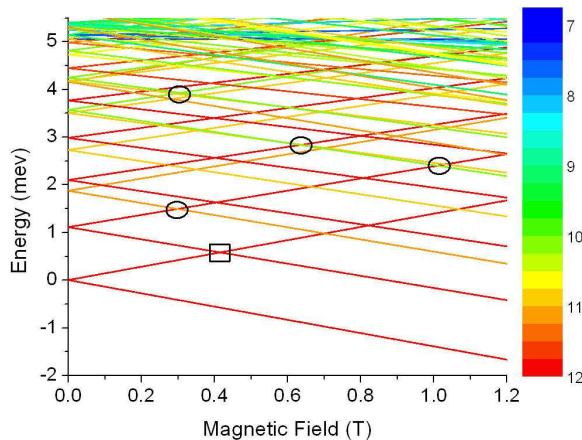


FIG. 7: Energy levels of the higher-barrier compound as a function of  $B$ , applied along the  $z$  axis. The color maps for each state the value of  $S_{eff}$ , where  $\langle S^2 \rangle := S_{eff}(S_{eff} + 1)$ . Ellipses and the square indicate representative examples of level crossings.

overlapping with the ground one implies that a magnetic field applied along the molecule's easy axis induces crossings involving states which are absent in a giant spin description. These can be turned into anticrossings (ACs) by the small transverse terms contained in  $H'$ . Figure 7 shows that besides the "traditional" intra- $S = 12$  crossings at about 0, 0.4 (e.g., the square) and 0.8 T, many more occur for intermediate values of  $B$ . In particular, there are three different kinds of "non-traditional" field-induced crossings, i.e., which are absent in the giant spin description of the molecule. First of all there are crossings involving a pair of states belonging to a single low-energy  $S$  multiplet different from the ground one (for instance the higher-lying ellipsis at 0.3 T in Fig. 7). These crossing may lead to relaxation shortcuts if the dominant relaxation path passes through them. The other two kinds of crossings (e.g. the other ellipses in Fig. 7) involve pairs of states belonging to different  $S$ -manifolds. The distinction arises from the symmetry properties of the two crossing states, i.e., they may have the same par-

ity or not. In the first case (e.g., the crossings between red and green curves in the two ellipses at about 0.6 and 1 T)  $H'$  usually leads to an AC, whereas in the second case (e.g., the ellipse at about 0.3 T) an AC may occur to the extent that at low  $T$  the inversion center is removed by a distortion, leading to terms with low-enough symmetry in  $H'$ . Even if there are no structural data below 150 K, it is not unlikely for magnetic molecules to undergo a symmetry lowering at low  $T$  (see, e.g., [10, 11]). "Non-traditional" ACs with the associated resonant incoherent tunneling, may result in relaxation shortcuts leading to additional steps in hysteresis cycles, absent in a giant-spin picture. For instance, Fig. 8 shows an example of derivative of the hysteresis curves measured at  $T = 3$  K for the higher-barrier molecule[3]. The "traditional" ACS produce minor features in these curves, and the two main peaks are associated with "non-traditional" ACs. The effect of low-field ACs is more evident at higher  $T$ [5]. For instance, there are features at 0.3 T which may a priori originate from both crossings marked on Fig. 7.

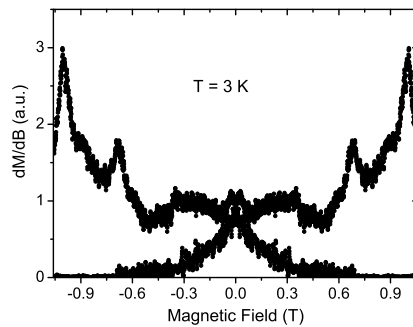


FIG. 8: Example of derivative of the hysteresis curves measured for the higher-barrier molecule in [3]. For each value of  $B$ , there are two points corresponding to increasing or decreasing  $B$  in the hysteresis cycle.

#### IV. CONCLUSIONS

By exploiting INS and FDMRS we have determined the microscopic Hamiltonian of two different high-spin variants of the  $Mn_6$  nanomagnet. We have found that excited  $S$  multiplets overlapping with the ground one strongly affect the magnetic relaxation process. Moreover, we have demonstrated the existence of tunnelling pathways involving pairs of states belonging to different total spin manifolds. Hence, the energy separation between the ground and excited multiplets may be a key ingredient in determining the relaxation and tunnelling dynamics of molecular nanomagnets.

- 
- [1] D. Gatteschi, R. Sessoli and J. Villain, *Molecular Nanomagnets*, Oxford University Press (2006).
  - [2] J. Villain, F. Hartmann-Boutron, R. Sessoli, and A. Rettori, *Europhys. Lett.* **27**, 159 (1994); A. Würger, *J. Phys.: Condens. Matter* **10**, 10075 (1998); M. N. Leuenberger and D. Loss, *Phys. Rev. B* **61**, 1286 (2000); D. Zueco and J. L. Garcia-Palacios, *Phys. Rev. B* **73**, 104448 (2006).
  - [3] C. J. Milios, A. Vinslava, W. Wernsdorfer, S. Moggach, S. Parsons, S.P. Perlepes, G. Christou and E.K. Brechin, *J. Am. Chem. Soc.* **129**, 2754 (2007).
  - [4] C. J. Milios, A. Vinslava, P. A. Wood, S. Parsons, W. Wernsdorfer, G. Christou, S.P. Perlepes and E.K. Brechin, *J. Am. Chem. Soc.* **129**, 8 (2007).
  - [5] S. Carretta, T. Guidi, P. Santini, G. Amoretti, O. Pieper, B. Lake, J. van Slageren, F. El Hallak, W. Wernsdorfer, H. Mutka, M. Russina, C. J. Milios and E. K. Brechin, *Phys. Rev. Letters* **100**, 157203 (2008).
  - [6] S. Carretta, E. Livioti, N. Magnani, P. Santini, and G. Amoretti, *Phys. Rev. Lett.* **92**, 207205 (2004).
  - [7] K. Blum, *Density Matrix Theory and Applications*, Plenum Press, NY (1996).
  - [8] P. Santini, S. Carretta, E. Livioti, G. Amoretti, P. Carretta, M. Filibian, A. Lascialfari and E. Micotti, *Phys. Rev. Lett.* **94**, 077203 (2005).
  - [9] S. Carretta, P. Santini, G. Amoretti, M. Affronte, A. Candini, A. Ghirri, I. S. Tidmarsh, R. H. Laye, R. Shaw, and E. J. McInnes, *Phys. Rev. Lett.* **97**, 207201 (2006).
  - [10] S. Carretta, J. van Slageren, T. Guidi, E. Livioti, C. Mondelli, D. Rovai, A. Cornia, A. L. Dearden, F. Carasughi, M. Affronte, C. D. Frost, R. E. Winpenny, D. Gatteschi, G. Amoretti and R. Caciuffo, *Phys. Rev. B* **67**, 094405 (2003).
  - [11] S. Carretta, P. Santini, G. Amoretti, T. Guidi, R. Caciuffo, A. Candini, A. Cornia, D. Gatteschi, M. Plazanet, and J. A. Stride, *Phys. Rev. B* **70**, 214403 (2004).